Title

Identification of and Structural Insights into Hit Compounds Targeting N-Myristoyltransferase for Cryptosporidium Drug Development

Journal

ACS Infectious Diseases, 9(10)

ISSN

2373-8227

Authors

Fenwick, Michael K

Reers, Alexandra R

Liu, Yi

et al.

Publication Date

2023-10-13

DOI

10.1021/acsinfecdis.3c00151

ACS Infectious Diseases

pubs.acs.org/journal/aidcbc
Article

Identification of and Structural Insights into Hit Compounds Targeting *N*-Myristoyltransferase for *Cryptosporidium* Drug Development

Michael K. Fenwick,[¶] Alexandra R. Reers,[¶] Yi Liu, Rachael Zigweid, Banumathi Sankaran, Janis Shin, Matthew A. Hulverson, Bradley Hammerson, Elena Fernández Álvaro, Peter J. Myler, Alexis Kaushansky, Wesley C. Van Voorhis, Erkang Fan,* and Bart L. Staker*

Cite This: *ACS Infect. Dis.* 2023, 9, 1821−1833

Read Online

ACCESS | Metrics & More | Article Recommendations | Supporting Information

ABSTRACT: Each year, approximately 50,000 children under 5 die as a result of diarrhea caused by *Cryptosporidium parvum*, a protozoan parasite. There are currently no effective drugs or vaccines available to cure or prevent *Cryptosporidium* infection, and there are limited tools for identifying and validating targets for drug or vaccine development. We previously reported a high throughput screening (HTS) of a large compound library against *Plasmodium N*-myristoyltransferase (NMT), a validated drug target in multiple protozoan parasite species. To identify molecules that could be effective against *Cryptosporidium*, we counter-screened hits from the *Plasmodium* NMT HTS against *Cryptosporidium* NMT. We identified two potential hit compounds and validated them against *Cp*NMT to determine if NMT might be an attractive drug target also for *Cryptosporidium*. We tested the compounds against *Cryptosporidium* using both cell-based and NMT enzymatic assays. We then determined the crystal structure of *Cp*NMT bound to Myristoyl-Coenzyme A (MyrCoA) and structures of ternary complexes with MyrCoA and the hit compounds to identify the ligand binding modes. The binding site architectures display different conformational states in the presence of the two inhibitors and provide a basis for rational design of selective inhibitors.

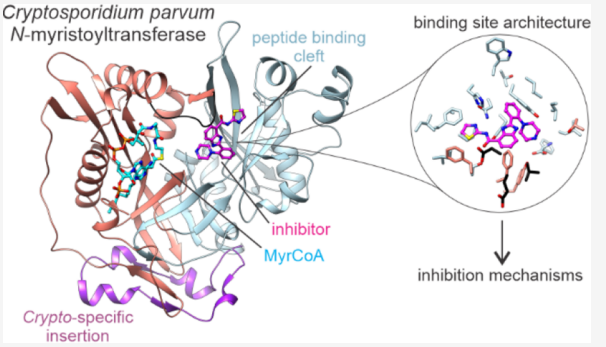

KEYWORDS: *Cryptosporidium, N-myristoyltransferase, drug discovery, childhood infectious disease*

INTRODUCTION

Children in developing countries are vulnerable to multiple health challenges including diseases associated with poor nutrition and contaminated water, with 500,000 annual deaths due to diarrheal diseases caused by infectious parasites (WHO[1]). In a three year prospective study of 20,000 children, the Global Enteric Multicenter Study (GEMS) found the four most prevalent infectious agents to be rotavirus, *Cryptosporidium*, *Escherichia coli*, and *Shigella*.[2] The most common non-viral diarrheal agent, *Cryptosporidium*, is a protozoan parasite in the same Phylum as the malaria-causing parasite *Plasmodium*. A Malnutrition and Enteric Disease (MAL-ED) study showed *Cryptosporidium* spp. to be among the top five pathogens in the first year of life of children with diarrhea.[3] *Cryptosporidium* showed increased prevalence in infants 0−11 months old and toddlers 12−23 months old; the highest mortality rates were associated with infants and toddlers with moderate-to-severe diarrhea.[4] An update to the GEMS study revealed continuing prevalence of *Cryptosporidium* in children 5 and under, peaking with infants and toddlers.[5] Additionally, an association has been found between *Cryptosporidium* infections (including asymptomatic infections) with growth cessation (stunting) and developmental delay in malnourished children.[6−8]

Medications for treatment of moderate-to-severe diarrhea in infants and toddlers remain severely lacking. While oral rehydration is an important therapy, the immune system of malnourished children is not able to clear the *Cryptosporidium* infection, so recurrence is chronic. The only FDA approved drug for the treatment of cryptosporidiosis, Nitazoxanide, has low effectiveness, especially among malnourished children with ongoing diarrhea, the children in most need of intervention.[9−11]

Cryptosporidia are difficult to culture beyond a few replication cycles, and extensive genomic studies regarding gene function and essentiality as a starting point for target-

Received: March 29, 2023
Published: September 18, 2023

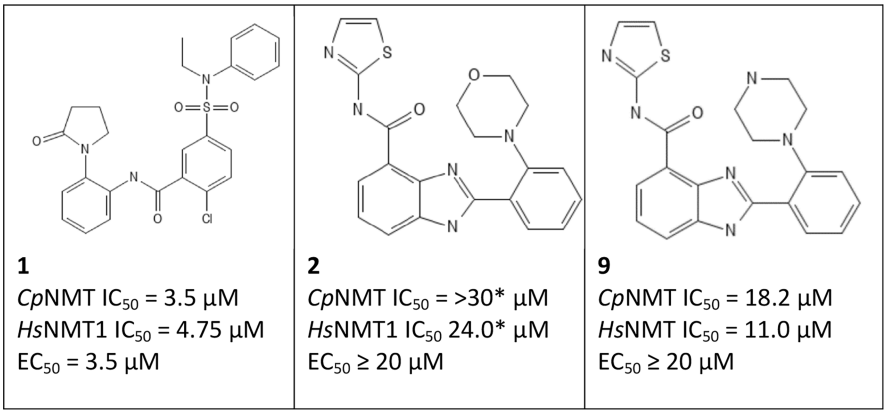

Figure 1. Hit compounds from screening. Chemical diagrams of hits from *Plasmodium* HTS[33] that show inhibition of *Cp*NMT (**1** and **2**). IC_{50} values against *Cp*NMT and *Hs*NMT are shown as well as EC_{50} values against *C. parvum* from compounds that were resynthesized as part of this work. *Compound **2** showed potential assay interference, failing to achieve 100% inhibition at high concentrations.

Scheme 1. Synthetic Route of Compound 9[a]

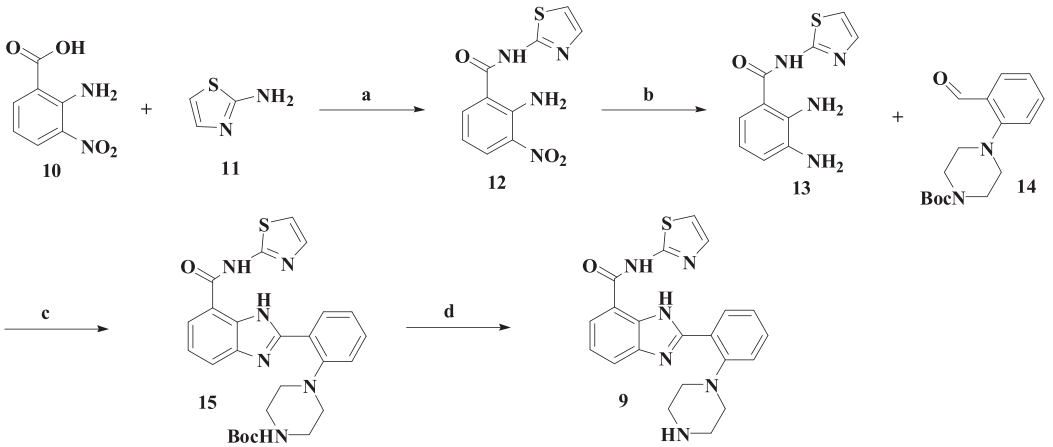

[a]Reagents and conditions: (a) EDCI, HOBT, DCM, rt., overnight; (b)10% Pd/C, H_2, MeOH/THF, overnight, 46% yield for two steps; (c) AcOH, microwave, 65 °C, 0.5 h, 76%; (d) TFA, 92%.

based drug development are lacking.[12−14] Phenotypic screening to identify *Cryptosporidium* killing compounds is challenging due to the need to access fresh oocysts from animals.[4,15−18] To identify compounds active against *Cryptosporidium*, we used a target repurposing approach investigating the potential drug target *N*-myristoyltransferase (NMT).

NMT catalyzes the transfer of myristate to an *N*-terminal glycine of substrate peptides following methionine removal.[19] Generally, it is held that myristoylation of substrate proteins is essential for protein−protein and protein−membrane interaction in the cell[20−23]—although the specific role of myristoylation in the context of protein−membrane interactions is yet to be determined.[24,25] For small molecule drug discovery, the peptide binding pocket of NMT specifically has been of interest as the sequence is not strictly conserved across species. NMT is both druggable and essential in *Trypanosoma cruzi*,[26] *Trypanosoma brucei*,[27] *Leishmania major*,[28] *Plasmodium falciparum*,[29] and *Plasmodium vivax*,[29−32] and thus identification of bioactive compounds against *Cryptosporidium* NMT presents an attractive opportunity for drug development.

As part of the GlaxoSmithKline (GSK) Tres Cantos Open Lab program, we participated in a screening campaign of the GSK library of 1.8 million compounds for inhibitory activity against *P. falciparum* NMT (*Pf*NMT) and *P. vivax N*-myristoyltransferase (*Pv*NMT).[33] This study identified 23 potential hit chemical scaffolds from the *Pv*NMT HTS, which showed selectivity over the human enzyme. We have recently begun testing the activities of some of these compounds against *Cryptosporidium parvum* NMT (*Cp*NMT). We assessed the potential of the compounds by measuring inhibition of the enzymatic activity of recombinant, purified *Cp*NMT using a fluorescence-based activity assay. We identified two of the compounds as inhibitors of *Cp*NMT and determined IC_{50} values against both human NMT (*Hs*NMT) and *Cp*NMT. We then determined the ability of the compounds to reduce infection in a cell-based model of *Cryptosporidium* infection. We also determined high-resolution crystal structures of *Cp*NMT bound to Myristoyl-Coenzyme A (MyrCoA) and ternary complexes with MyrCoA and two of the hit compounds at 2.20, 1.90, and 2.0 Å resolution, respectively. The results show that *Cp*NMT is a viable target that can be accessed in cells and provide structural details of the mechanism of inhibitory action of the molecules.

RESULTS AND DISCUSSION

Enzymatic Assay Optimized *Z′* at pH 7.0. We focused on two hit compounds from the HTS against *Plasmodium* NMT, referred to here as compounds **1** and **2**, that showed

https://doi.org/10.1021/acsinfecdis.3c00151
ACS Infect. Dis. 2023, 9, 1821−1833

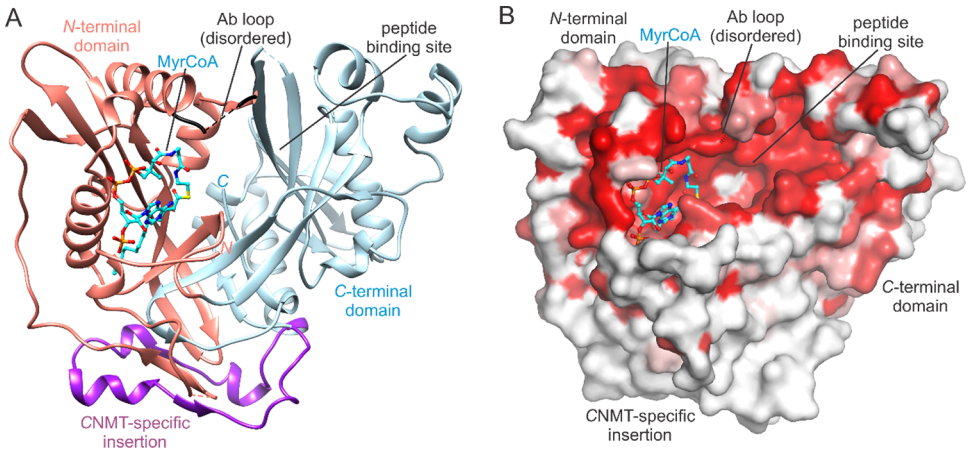

Figure 2. Crystal structure and conservation of *Cp*NMT. (A) Overall structure of *Cp*NMT-K310A-E311A (ribbons) bound to MyrCoA (cyan, balls-and-sticks). The structure displays the NMT fold, with an NMT *N*-terminal domain, truncated for crystallization (salmon, residues 39−218), and an NMT *C*-terminal domain (light blue, residues 219−466) that contains an insertion unique to the NMTs of *Cryptosporidia* (purple, residues 289−329). The Ab loop (black, residues 109−116) is partially disordered. (B) Amino acid conservation. Conservation is depicted according to the coloring scheme of ENDscript 2.0[46] with default parameter values (white, lack of conservation; red, identity) mapped onto the solvent-accessible surface.

inhibition of *Cp*NMT (Figure 1). To measure the inhibition activities, we modified an *N*-myristoylation assay developed by Goncalves et *al.*[34] for human NMTs and utilized previously for screening compounds against *Lm*NMT,[35] *Pv*NMT,[36] and *Pf*NMT.[33] In our hands, the original assay[33] yielded high background readings, possibly due to the spontaneous reaction of thiol and maleimide. The maleimide-thiol reaction is highly sensitive to pH and favors sulfhydryl groups at pH 6.5−7.5. We decided to test enzymatic conditions by varying the pH between 6.0 and 8.5. To measure the reliability of the assay, Z' was used as a parameter of assay quality.[37] Z' factors between 0.8 and 1.0 reflect reliable high throughput assays. As illustrated in Figure S1, Z′ is the highest at pH 7.0, showing a value of 0.84 ± 0.08 at a 30 min cutoff up to which point a linear reaction with time was observed. Using pH 7.0 together with 25 nM *Cp*NMT, 10 μM *Pf*ARF-peptide (Methods), 10 μM MyrCoA, and 8 μM CPM, the K_M values were determined to be 0.42 ± 0.13 μM for MyrCoA and 3.53 ± 0.69 μM for *Pf*ARF at saturating concentrations of *Pf*ARF-peptide and MyrCoA, respectively. The *Pf*ARF-peptide is derived from the *N*-terminal sequence (aa2−16) of the *P. falciparum* ADP-ribosylation factor, a known NMT substrate in multiple species.[33,34]

Two Hit Compounds from *Plasmodium* NMT HTS Active against *Cryptosporidium NMT*. Compounds **1** and **2** showed inhibition of the *Cryptosporidium* enzyme when tested at 30 μM. To verify inhibition, we conducted dose response studies and determined IC_{50} values (Figure 1). Compound **2** showed dose-dependent inhibition; however, 100% inhibition was not achieved even at 30 μM, suggesting potential assay interference at high concentrations of the compound and a potential false positive screening hit. We also synthesized a modified version of **2** replacing the morpholine group with a piperazine moiety (Compound **9**; Scheme 1 and Figures S2 and S3), anticipating higher affinity based on known inhibitors of NMT that show a preference for ammonium group interaction with the *C*-terminal carboxylate.[29,31,38]

Compound 1 Shows Antiparasite Activity in Cell-Based Assays. To further determine if compounds were active against live parasites in culture, we tested their ability to inhibit the growth of parasites on human colorectal adenocarcinoma cells (HCT-8). We found that compound **1**, but not **2** or **9**, inhibits growth of parasite on HCT-8 cells (Figure 1). Our previous experience comparing target-based screens to cell-based assays suggests that IC_{50} less than 2 μM is necessary to see growth inhibition, thus it is not surprising that the low affinity inhibitors did not show inhibition in this assay.[39]

Crystallizable Constructs of *Cp*NMT Provide A Platform for Structure-Guided Inhibitor Development. We performed a screening of *Cp*NMT constructs to identify ones that could be overexpressed and used to generate high-resolution co-crystal structures of the enzyme bound to the inhibitors (Supplementary Methods and Tables S1 and S2). We produced one construct comprising hexahistidine fusion tagged *Cp*NMT (B1, Table S1), 11 constructs of *Cp*NMT with *N*-terminal truncations and cleavable fusion tags (A2−A12 in Table S1 and Figure S4), and two variants of construct A4 that additionally contain one or two alanine substitutions of surface residues designed using surface entropy reduction methods[40] (A41 and A42, respectively, Table S1). Preparations of the tag-free form of construct A10, which corresponds to a deletion of residues 1−39, yielded crystal structures of the ternary complexes of *Cp*NMT, MyrCoA, and hit compounds **1** and **9** that were refined to resolutions of 1.90 and 2.00 Å, respectively (Tables S3 and S4). In addition, the cleaved form of construct A42, which corresponds to a deletion of residues 1−38, was used to obtain a co-crystal structure of *Cp*NMT and MyrCoA that was refined to 2.20 Å. Composite omit maps validating ligand binding are illustrated in Figure S5.

The crystal structures belong to space group $P2_1$ and have two copies of the enzyme in the asymmetric unit. However, the unit cell dimensions and packing arrangements of the *Cp*NMT molecules differ significantly between the inhibitor-free and inhibitor-bound crystal structures (Table S3 and Figure S6). Analysis of surfaces and interfaces within the crystals suggests a monomeric biological assembly, confirming results from size exclusion chromatography.

In the crystal structures of *Cp*NMT bound to **1** and **9**, the two asymmetric chains are more similar conformationally to

https://doi.org/10.1021/acsinfecdis.3c00151
ACS Infect. Dis. 2023, 9, 1821−1833

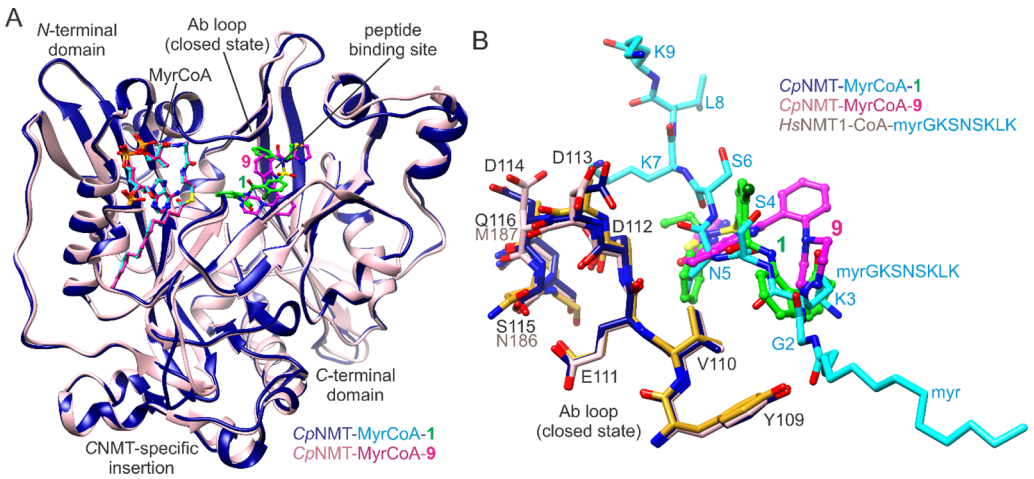

Figure 3. Structural basis of *Cp*NMT inhibition by repurposed hit compounds. (A) Compounds **1** and **9** bind a similar region of the peptide binding cleft. Structural superpositions are based on *Cp*NMT *Cα* atoms. (B) The inhibitors block the binding of peptide residues 3−6, as suggested by structural superpositions with *Hs*NMT1 bound to myristoylated NCS1 peptide (goldenrod and cyan, PDB entry 5O9S[51]). Complexation with **1** or **9** stabilizes the closed state conformation of the Ab loop.

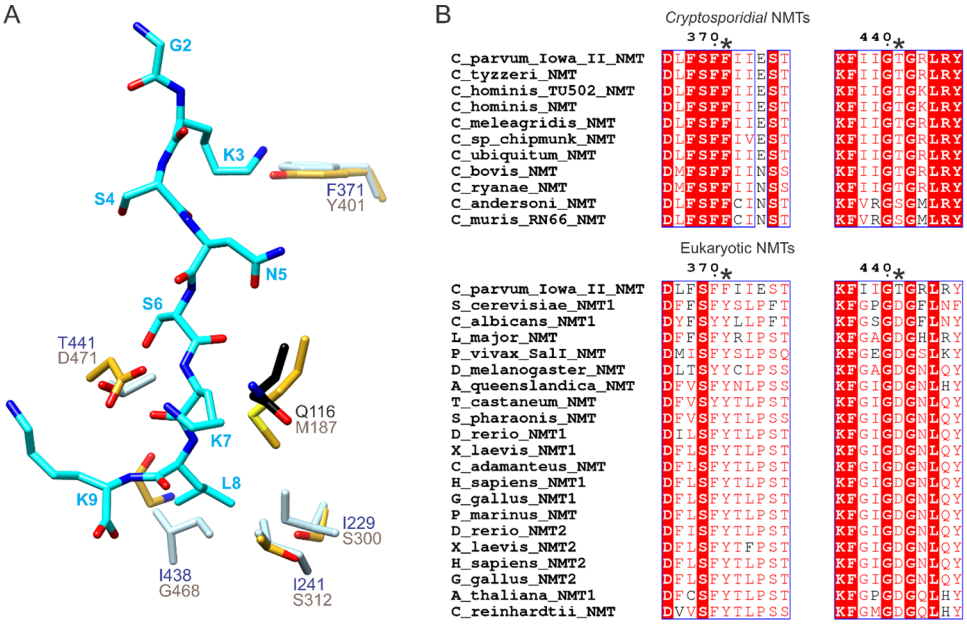

Figure 4. Unique amino acid usage within the peptide binding cleft of *Cp*NMT. (A) Nonconservative replacements of aligned residues of *Hs*NMT1 (represented as in Figure 3B) occur at the putative binding sites of peptide residues 3, 6, 7, and 8. (B) Phe371 and the hydroxyl group of Thr441 are conserved in *Cryptosporidium* NMTs, but are substituted by tyrosine and aspartate, respectively, in other eukaryotic NMTs. The amino acid sequence of *C. parvum* (Iowa II strain) NMT is aligned with those of *Cryptosporidium* (top) and other eukaryotic (bottom) orthologs (Methods).

the corresponding chains in the other structure than to their asymmetric unit mates, which can be attributed to crystal packing artifacts (Figure S7A,B). The artifacts do not affect the ability of **1** to bind to both asymmetric unit chains but result in small conformational differences near the ethyl side chain of **1** and in residues Phe240 and Thr441 (Figure S7C). In contrast, the differences in chain conformations accommodate the binding of **9** to chain A but not to chain B, possibly because this would lead to steric clashes between the thiazole moiety of **9** and the side chain of Phe240.

The crystal structure of *Cp*NMT bound to MyrCoA is less ordered than those containing **1** and **9**. Seventeen residues of chain A and 11 residues of chain B, many of which form part of the peptide binding cleft, were not modeled due to weak electron density. In addition, MyrCoA bound to chain B is only partially ordered (average B-factor of 86.0 Å^2, Figure S5F). The two surface residues mutated to facilitate crystallization make weak interactions with Asn46 and Thr47 of a symmetry-related chain and likely do not introduce structural artifacts. In contrast, all residues after Lys40 in the structures of *Cp*NMT bound to inhibitors were built into electron density, and the electron density of the modeled ligands is clearly defined. Thus, we anticipate that these constructs will be useful for the study of enzyme−inhibitor interactions at high resolution and conformational changes that accompany inhibitor binding.

Inhibitors Bind, and Order, the Peptide Binding Cleft of *Cp*NMT. *Cp*NMT bound to MyrCoA displays the NMT fold with conserved *N*- and *C*-terminal NMT domains (Figure 2A). PDBeFOLD[41] identified as having highly related folds (*Z*-

https://doi.org/10.1021/acsinfecdis.3c00151
ACS Infect. Dis. 2023, 9, 1821−1833

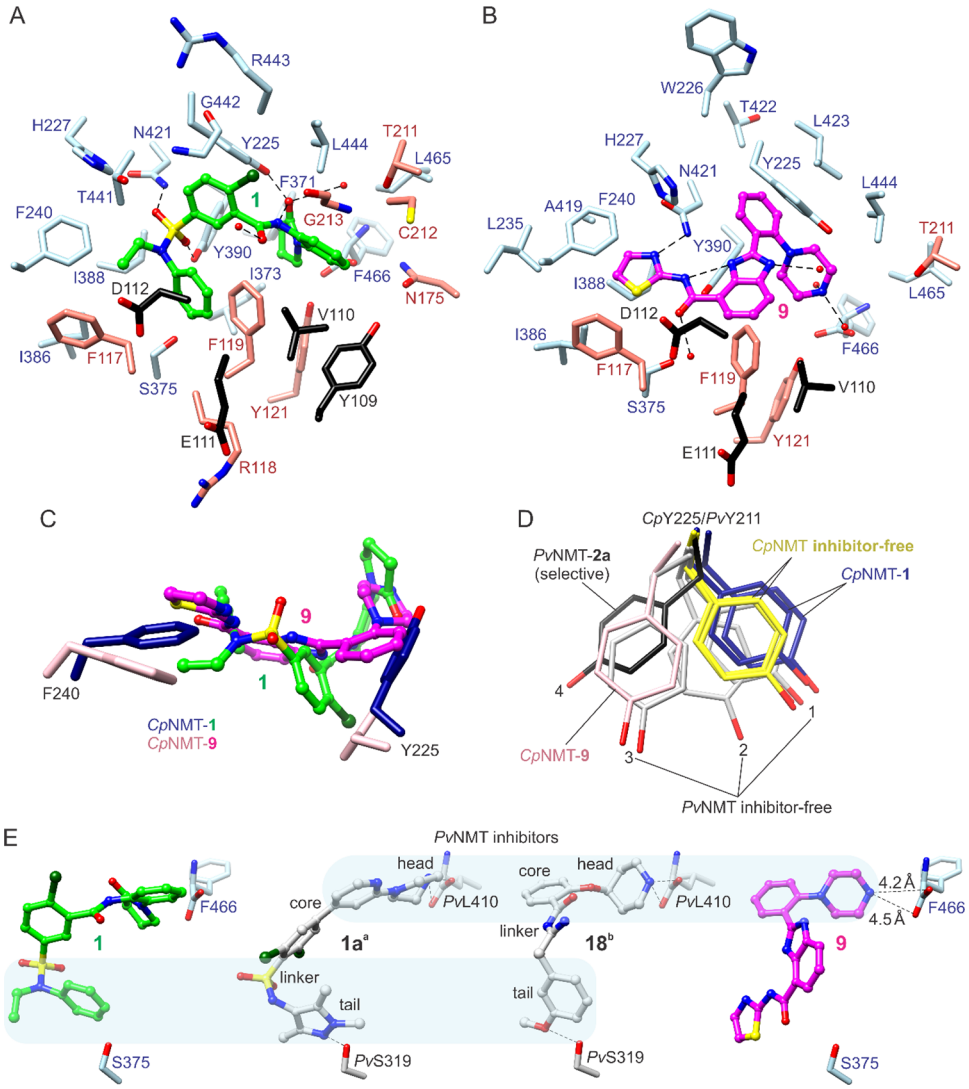

Figure 5. Inhibitor binding sites and target interactions for increasing potency. (A, B) Inhibitor binding sites. (A) Compound **1**. (B) Compound **9**. Residues within 5 Å of the inhibitors are colored as in Figure 2A. Hydrogen bonds are shown as dashed lines and water molecules as red spheres. (C) Compound **9** binds a rotated side chain conformation of Tyr225 and packs beneath Phe240. (D) Comparison of Tyr225 side chain rotamers with four rotamers of *Pv*Tyr211, including selective rotamer 4 (PDB entries 4B10 and 2YNE).[29,31] (E) Similarities of structures and binding modes of **1** and **9** with those of optimized *Pv*NMT inhibitors **1a**[29] [2,6-dichloro-4-(2-piperazin-1-ylpyridin-4-*yl*)-*N*-(1,3,5-trimethyl-1*H*-pyrazol-4-*yl*)benzenesulfonamide] and **18**[52] [*N*-[2-(3-methoxyphenyl)ethanimidoyl]-2-piperidin-4-yloxy-benzamide] suggest target hydrogen and ionic bonding interactions (dashed lines) for inhibitor optimizations. a, ref 29; b, ref 52.

scores >11) the chains of all of the NMT orthologs currently available in the PDB, including those of human, *P. vivax*, *L. major*, and *Leishmania donovani*, *Asperigillus fumigatus*, *Saccharomyces cerevisiae*, and *Candida albicans*. The RMSDs range from 1.19 Å (*Pv*NMT, PDB entry 4B11) to 1.68 Å (*Ca*NMT, PDB entry 1NMT). A water channel runs through the *C*-terminal domain containing several waters similarly positioned to ones observed in crystal structures of human NMTs that have been hypothesized to occupy a secondary myristoyl group binding site.[42−44] Notably, unlike the orthologous structures, the *C*-terminal domain of *Cp*NMT contains a unique 41 residue insertion (residues 289−329) located at the protein surface on the side opposite that of the peptide binding cleft (Figure 2A). The insertion comprises a large loop rich in secondary structure that extends β-sheets of the NMT fold. Also, α- and 3_{10}-helices within the loop bind a part of the *N*-terminal domain that encloses the myristoyl group binding site. The loop is similarly located to, and envelops after superposition, a 21-residue helix−loop−helix motif inserted within the *N*-terminal domains of *Leishmania* NMTs.[27,45]

Structure-based sequence alignments with orthologs using ENDSCRIPT show that the MyrCoA and putative peptide binding sites exhibit a high degree of amino acid conservation (Figure 2B). In the inhibitor-free structure, the well-characterized Ab loop[47,48] (residues 109−116) and the adjacent β-hairpin loop (residues 378−384) are partially disordered. Upon binding of **1** or **9**, these regions become highly ordered, reconstituting the peptide and MyrCoA binding sites, with the Ab loop in the closed conformation (Figure 3A,B). The inhibitors are predicted to block the binding of residues 3−6 of peptide substrates (Figure 3B), consistent with our repurposing predictions based on *Pv*NMT inhibitors, which typically bind the corresponding region of the peptide binding cleft of *Pv*NMT.[29,31−34,49,50]

https://doi.org/10.1021/acsinfecdis.3c00151
ACS Infect. Dis. 2023, 9, 1821−1833

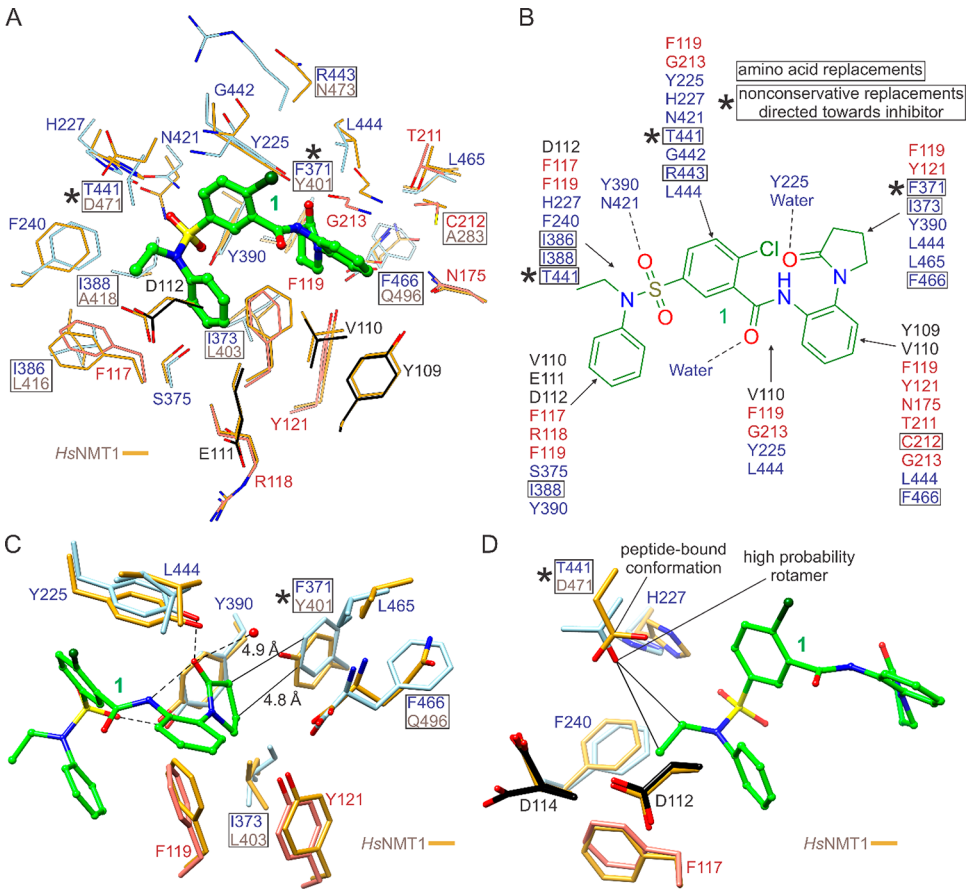

Figure 6. Strategies to produce selective inhibitors using the compound **1** series. (A) Conservative and nonconservative substitutions of aligned residues of *Hs*NMT1 (goldenrod, PDB entry 3IU1) in the binding site of **1** (boxed). Asterisks indicate nonconservative replacements having side chains directed toward the inhibitor. (B) Accompanying 2D schematic representation. (C, D) Potential target interactions. Panel (C) suggests modification of the γ-lactam to introduce closer contacts with the phenyl ring of Phe371 and steric clashes with Tyr401 of *Hs*NMT1. Panel (D) suggests modification of the ethyl side chain to form a hydrogen bond with Thr441 and not Asp471 of *Hs*NMT1 (shown in the peptide bound conformation; PDB entry 5O9S).[51]

Comparisons with the aligned residues of *Hs*NMT1 bound to a peptide show nonconservative replacements at the binding sites of substrate residues 3, 6, 7, and 8 (Figure 4A). At these sites, a phenylalanine substitutes for a tyrosine (*Cp*Phe371/*Hs*Tyr401), a threonine for an aspartate (*Cp*Thr441/*Hs*Asp471), a glutamine for a methionine (*Cp*Gln116/*Hs*Met187), and three isoleucines for two serines and a glycine (*Cp*Ile229/*Hs*Ser300, *Cp*Ile241/*Hs*Ser312, and *Cp*Ile438/*Hs*Gly468), respectively. Remarkably, Phe371 and the hydroxyl group of Thr441 are conserved in *Cryptosporidium* NMTs, whereas *Hs*Tyr401 and *Hs*Asp471 are strongly conserved in many other eukaryotic NMTs (Figure 4B). Thus, these differences might be leveraged for the development of selective *Cp*NMT inhibitors, including potentially peptidomimetic inhibitors.

Inhibitors Bind Alternate Conformations of the Peptide Binding Cleft. The inhibitor binding site architectures provide a molecular basis for the micromolar binding affinities of **1** and **9** for *Cp*NMT. Both compounds fold around the side chain of Phe119 (*Pv*Phe105) and make extensive hydrophobic interactions with residues of the two NMT domains, including the Ab loop (Figure 5A,B; see also schematics in Figures 6B and 7B). The bound conformations of both compounds contain an intramolecular hydrogen bond involving the core amide group, which is shared with the γ-lactam in the case of **1**, and the benzimidazole in **9** (Figure 5A,B). In the complex with **1**, three inhibitor−enzyme hydrogen bonds are formed by the sulfamoyl oxygens and the side chains of Tyr390 and Asn421 and by the γ-lactam oxygen and the side chain of Tyr225. In contrast, the complex with **9** displays only a single hydrogen bond, which is formed by the thiazole nitrogen and the side chain of Asn421.

The bound pose of compound **1** coincides somewhat closely with a superimposed peptide (Figure 3B). In contrast, **9** packs beneath the side chains of Tyr225 and Phe240 (Figure 5C). This causes the side chain of Tyr225 to rotate ∼40° relative to the ground state conformation observed in the inhibitor-free structure, to a state that matches closely rotamer 3 of a set of 4 observed *Pv*Tyr211 rotamers (Figure 5D).[29,31] Phe240 resides within a flexible loop formed by residues 238−248 and is largely disordered in the structure of inhibitor-free *Cp*NMT. In the complexes with **1** and **9**, Phe240 is more ordered near the inhibitor and adopts either an "in" or "out" conformation in the two asymmetric unit chains (Figure S7C). In the "out" state, a hydrophobic sub-pocket is accessible and forms part of the binding site of the thiazole group of **9**. In crystal structures of *Pv*NMT, a similar hydrophobic pocket is formed through conformational changes induced by some *Pv*NMT inhibitors having bulky tail groups.[53,33]

https://doi.org/10.1021/acsinfecdis.3c00151
ACS Infect. Dis. 2023, 9, 1821−1833

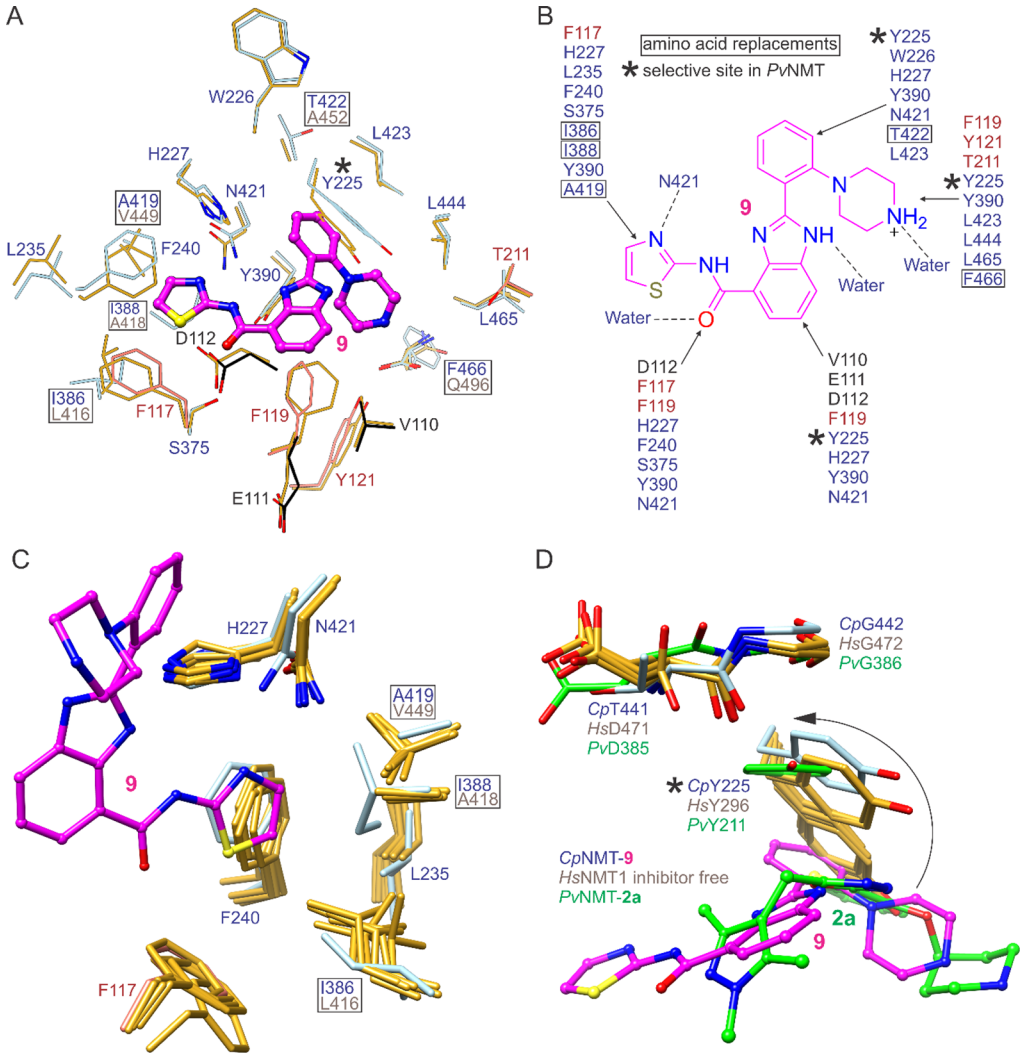

Figure 7. Strategies to produce selective inhibitors using the compound **9** series. (A) Conservative and nonconservative substitutions in the binding site of **9** (boxed). Tyr225 (asterisk) is a selective residue in *Pv*NMT. (B) Accompanying 2D schematic representation. (C) Structural differences in the thiazole binding site compared to *Hs*NMT1 create a potential target site for selective binding of optimized inhibitors to *Cp*NMT. (D) Binding modes of selective *Pv*NMT inhibitors, such as that of compound **2a** (green; PDB entry 2YNE[29]), suggest *Cp*NMT inhibitor optimizations that stabilize a more significant rotation of Tyr225. In panels (A), (C), and (D), aligned residues of *Hs*NMT1 are colored goldenrod (PDB entry 3IU1 in panel (A), and entries 3IU1, 5NPQ, and 5UUT[59] in panels (C) and (D)).

There are currently no co-crystal structures available of **1** and **9** bound to *Plasmodium* NMTs. However, it is noteworthy that a few of the inhibitor functional groups are structurally similar and bind similar subsites to moieties within particular *Pv*NMT inhibitors, such as compounds **1a** and **18** of refs 29 and 52, respectively. The core moieties of these *Pv*NMT inhibitors have an attached head group that forms an ionic bond with the C-terminal carboxylate of *Pv*Leu410 (*Cp*Phe466) and a tail group that forms a hydrogen bond with *Pv*Ser319 (*Cp*Ser375) (Figure 5E). The structural similarities thus suggest that a hydrogen bond acceptor might be introduced into **1** to recapitulate the hydrogen bonding interaction at the *Cp*Ser375 (*Pv*Ser319) site, and the electrostatic contacts made with Phe466 might be optimized by altering the head group and/or adjusting its spacer length.

Opportunities for Design of Selective Inhibitors. The inhibitor binding site of *Cp*NMT has several unique residues in comparison to those of human NMTs, which might provide some advantages for selective inhibitor development over other NMT inhibitor binding sites such as those of *Plasmodium* and *Leishmania* NMTs.[27,29−33,36,45,49,54−57] Within the binding site of **1**, Phe371 and Thr441 are potential target binding sites for achieving selectivity over *Hs*NMTs because they direct their side chains toward the inhibitor and there are nonconservative replacements in *Hs*NMTs (Figure 6A,B). In *Hs*NMT1, these residues are substituted by Tyr401 and Asp471, respectively. Tyr401 is located at the base of a conserved water channel and its function is unknown.[43,44] However, a co-crystal structure with the human NCS1 peptide shows that its hydroxyl group is positioned within the hydrogen bonding distance of the ε-amino group of NCS1 Lys3 (Figure 4A).[51] If Phe371 of *Cp*NMT cannot be mutated without loss of function, optimizations of inhibitors that lead to closer contacts with this residue but that clash with the hydroxyl group of *Hs*Tyr401 could potentially be a promising route to increased selectivity (Figure 6C).[58]

The corresponding residue of *Cp*Thr441 in *Hs*NMT1 and *Hs*Asp471 together with *Hs*Gly472 undergo a peptide flip isomerization that leads to hydrogen bonding with residues 6 and 7 of the peptide substrate.[51] If, like *Hs*Asp471, *Cp*Thr441

https://doi.org/10.1021/acsinfecdis.3c00151
ACS Infect. Dis. 2023, 9, 1821−1833

can orient its side chain into the peptide binding cleft to form hydrogen bonding interactions with the substrate, the ethyl side chain of **1** might be altered to bind the hydroxyl group selectively through the addition of a hydrogen bond acceptor (Figure 6D).

Within the binding site of **9**, there are no target residues in close proximity to the inhibitor on the basis of nonconservative replacements and side chain orientations (Figure 7A,B). Redesign of the piperazine head group, which is greater than 6 Å from Phe371, would thus be required to selectively bind that residue. The thiazole binding site might also be targeted for selectivity because it includes a hydrophobic pocket containing three substitutions (*Cp*Ala419/*Hs*Val449, *Cp*Ile388/*Hs*Ala418, and *Cp*Ile386/*Hs*Leu416) that change the van der Waals surface (Figure 7C). The *Cp*Ile388/*Hs*Ala418 substitution also influences the side chain conformation of *Cp*Asn421/*Hs*Asn451.

Tyr225 is an additional potential target site for selective binding if it shows a difference in rotameric preferences relative to Tyr296 of *Hs*NMT1. This strategy has been employed to achieve selective inhibition of *Pv*NMT on the basis of a highly rotated conformation of *Pv*Tyr211 adopted in complexes with selective inhibitors.[29−32] In contrast, the side chain of *Cp*Tyr225 does not rotate to the same degree in response to the binding of **9**, and *Hs*Tyr296 is able to adopt a similar rotamer in the absence of inhibitors (Figure 7D). Thus, selectivity might be increased through inhibitor modifications that cause greater rotation of this residue.

CONCLUSIONS

In this study, we demonstrated the ability to inhibit *Cp*NMT by repurposing a selection of hits from an HTS of compounds against *Plasmodium* NMTs. In addition, we identified crystallization constructs that can be used to produce high-resolution crystal structures of *Cp*NMT bound to MyrCoA and hit compounds, thus setting the stage for future structure-aided inhibitor development. While this study focused on the repurposing of non-peptidomimetic hits, substrate mimetic inhibitors of *Cp*NMT might also be considered in the future given the unique amino acid usage at many sites within the peptide binding cleft. From the HTS compounds, we identified two hits against *Cp*NMT and validated them through enzymatic and structural studies. Inspection of the X-ray crystal structures of the inhibitor-bound complexes suggests strategies for increasing inhibitor affinity and selectivity. We aim to focus our molecular designs to optimize hydrophobic contacts to Phe371, which are likely to clash with the hydroxyl group of the homologous Tyr401 of the human enzyme. This strategy, combined with optimizations to induce the mobile Tyr225 to be in a "selective" conformation, represents a promising additive approach to improve inhibitor selectivity and affinity.

METHODS

Enzymatic Assay. The synthetic peptide Gly-Leu-Tyr-Val-Ser-Arg-Leu-Phe-Asn-Arg-Leu-Phe-Gln-Lys-Lys-NH2 derived from the *N*-terminal sequence (amino acids 2−16) of *P. falciparum* ADP-ribosylation factor (*Pf*ARF) was purchased from Innopep (San Diego, California). 7-Diethylamino-3′(4′-maleimidylphenyl)-4-methylcoumarin (CPM) and MyrCoA were purchased from Thermo Scientific Life Technologies (Grand Island, New York) and Med Chem 101 LLC (Plymouth Meeting, Pennsylvania), respectively.

The inhibition assay was adapted from Goncalves et *al.*[34] The assay buffer was prepared in a 4× stock solution consisting of 9.2 mM potassium phosphate, 69.7 mM sodium phosphate, 2 mM EDTA, and 10% TritonX-100 at pH 7.0. Working stock solutions were made fresh, adding DMSO to final concentrations of either 1 or 5% (v/v). The *Cp*NMT enzyme was diluted in assay buffer containing 1% DMSO to a final concentration of 25 nM.

Ten μL of the test compound or 10% DMSO in lieu of compound was dispensed into a 96-well plate (Greiner Bio-One), and 50 μL of enzyme (in assay buffer containing 1% DMSO) was added to a final concentration of 25 nM per well. The plate was incubated for 30 min at room temperature. The enzymatic reaction was initiated by adding 50 μL of reaction substrates containing 10 μM MyrCoA and *Pf*ARF-peptide as well as 8 μM CPM. Fluorescence readings were taken on a Spectra M2 plate reader (Molecular Devices) with excitation and emission wavelengths of 385 and 485 nm, respectively. Fluorescence intensities were measured in 1 min intervals for 45 min. Background fluorescence and noise were determined by replacing each constituent of the reaction individually with assay buffer containing 1% DMSO, and values were deducted from experimental sample values. The pH of the assay buffer was varied between 6.0 and 8.5 to determine optimal reaction conditions with minimal background and off target reactions. A linear reaction rate was observed during the first 30 min and used to determine all values. The Michaelis−Menten constants (K_M) for *Pf*ARF-peptide and MyrCoA were determined at saturating concentrations of the respective co-substrates. Experiments were carried out in triplicate. Data from the primary screen, confirmation screen, and dose−response experiments were analyzed with Graphpad Prism. For IC_{50} determination, dose−response curves were fitted using Graphpad Prism best fit values from log(inhibitor) vs response−variable slope (four parameters), GraphPad Software, San Diego, California.

EC_{50} *Cryptosporidium* Whole Cell Activity. Compounds and the Iowa strain of *C. parvum*, expressing Nluciferase (Nluc), were added to confluent lawns of HCT-8 cells in 384-well plates.[60] The luciferase signal amplified 10−40-fold after 72 h in the absence of drug; each well was examined microscopically for integrity of the HCT-8 cells. Wells containing bioactive compounds that inhibited *C. parvum* growth showed only a fraction of the luminescence (<10%) of the wells containing the solvent alone.

Cloning and Construct Optimization. Cloning as well as protein production and crystallization were conducted at the SSGCID[61,62] following standard protocols described previously.[63−65] Genomic DNA from *C. parvum* strain Iowa II was purchased from ATTC. To grow crystals of *Cp*NMT, we created a series of gene variants of *Cpnmt* (Gene ID cgd3_320, Uniprot accession code Q5CV46), including ones encoding *N*-terminal truncations and mutations of charged surface residues based on the surface entropy prediction server.[40] Primers are listed in Table S2, and the expressed enzyme products, together with observations of crystallization and diffraction, are reported in Table S1. Protein expression and crystallization of the various constructs were conducted as described in the sections below.

The truncations were created by PCR amplification using Platinum SuperFi PCR Master Mix according to the

https://doi.org/10.1021/acsinfecdis.3c00151
ACS Infect. Dis. 2023, 9, 1821−1833

manufacturer's protocol. Amplicons were gel-purified (Machery-Nagel), and gene fragments were ligated into the ligation independent cloning (LIC)[66] expression vector pAVA0421[64] encoding a cleavable 6xHis fusion tag followed by the human rhinovirus 3C protease-cleavage sequence (MAHHHHHHMGTLEAQTQGPGS-ORF). For the ligation reaction, the digested vector and the gene fragments were incubated at 50 °C for 30 min and inserted at restriction sites *PmeI* and *NruI* using NEBuilder HiFi DNA Assembly master mix (New England BioLabs, Ipswich, MA). Plasmids were stored in NEB5-alpha cells (New England BioLabs, Ipswich, MA). Codon variants encoding surface mutations added to the truncation constructs were generated using the QuikChange Lightning Site-Directed Mutagenesis Kit (Agilent) according to the manufacturer's protocol. The resulting plasmids were stored in TOP10 cells.

Protein Expression and Purification. Chemically competent *E. coli* Rosetta 2 (DE3) cells were transformed with plasmids pAVA0421 encoding the various *Cp*NMT gene constructs. Cells were expression-tested, and 4−12 L of culture was grown using auto-induction media[67] in the LEX bioreactor for 18−22 h at 18 °C. Expression clones were assigned the SSGCID target identifier prefix CrpaA.18219.a (Table S1) and are available at https://www.ssgcid.org/available-materials/ssgcid-proteins/.

*Cp*NMT variants were purified using a five-step protocol consisting of immobilized metal (Ni^{2+})-affinity chromatography (IMAC), anion exchange chromatography (AEX), cleavage of the *N*-terminal hexahistidine tag, passage over a second Ni^{2+} affinity column, and size-exclusion chromatography (SEC). All chromatography runs were performed on an ÄKTA purifier 10 (GE Healthcare) using automated IMAC and SEC programs according to previously described procedures.[63] Fractions collected from the IMAC column were concentrated, diluted 100-fold in AEX buffer (20 mM Bis-tris propane, 1 mM TCEP, pH 9.7), and applied to HiTrap Q columns (GE Healthcare). For the constructs with truncations, including ones also having the surface mutations, appropriate buffers for the AEX column were selected based on the theoretical isoelectric points. Fractions were eluted using a linear gradient of AEX buffer, with NaCl endpoint concentrations of 25 and 500 mM over five column volumes. Fractions containing *Cp*NMT were pooled, and *N*-terminal 6xHis tag removal was achieved by the addition of His-MBP-3C protease (1:50, protease:protein) and overnight incubation at 4 °C in dialysis buffer (25 mM HEPES, pH 7.5, 500 mM NaCl, 5% glycerol, 1 mM TCEP, and 0.025% sodium azide). Untagged NMT was recovered by applying the dialysate to a second IMAC column. SEC was performed on a HiLoad 26/600 Superdex 75 pg column (GE Healthcare) using a mobile phase of 20 mM HEPES, 300 mM NaCl, 5% glycerol, and 1 mM TCEP, pH 7.0. TCEP was omitted from the mobile phase for protein utilized in the enzyme activity assays. Peak fractions eluted as a single peak at a volume consistent with a monomeric assembly and were pooled and analyzed for the presence of the protein of interest using sodium dodecylsulfate polyacrylamide gel electrophoresis. The peak fractions were concentrated to 36.5 mg/mL using an Amicon purification system (Millipore). Aliquots were flash-frozen in liquid nitrogen and stored at −80 °C.

Crystallization. All purified constructs of *Cp*NMT described in Table S1 were prepared for crystallization studies following previously described protocols used for *L. major* NMT.[27,38] Samples were first incubated with 1 mM MyrCoA at room temperature for 20 min. For co-crystallizations with inhibitors, the inhibitors were also added at concentrations of 1 mM prior to incubation. MyrCoA and compound stock solutions were prepared in 100% DMSO, and when combined with protein solutions, the final DMSO concentrations did not exceed 3%. Protein−ligand mixtures were screened for crystallization in 96-well sitting-drop plates against the JCSG ++ HTS (Jena Bioscience) and Morpheus HT96 (Molecular Dimensions) crystal screens. Drops containing equal volumes (0.5 μL) of protein and precipitant solutions were prepared at room temperature next to reservoir solutions (80 μL) in sitting-drop vapor-diffusion format.

Both constructs B1 and tag-free A4 crystallized. However, the crystals of B1 did not diffract, and the highest resolutions of X-ray reflections obtained for crystals of A4 were ∼3.5 Å. Crystals suitable for structure determination of *Cp*NMT bound to MyrCoA, and *Cp*NMT bound to MyrCoA and compound **1** or **9**, were grown using constructs A42 (residues 39−466, K310A/E311A) and A10 (residues 40−466), respectively. Crystals of *Cp*NMT-MyrCoA appeared after 72 h in wells containing JCSG+ condition H3 and were harvested after 3 to 4 weeks. Crystals were looped and flash-frozen via plunging directly into liquid nitrogen with addition of ∼25% PEG400 as a cryo-protectant. Final crystallization conditions for both binary and ternary complexes were 100 mM Bis-Tris−HCl, pH 5.5−6.5, 25−27.5% PEG 3350.

X-ray Data Collection, Structure Determination, and Refinement. Frozen crystals were shipped to the Advanced Light Source (ALS), Berkeley National Laboratory, as part of the Collaborative Crystallography program of ALS-ENABLE. Data were collected at 100 K on ALS-ENABLE beamlines as described in Table S3. Raw X-ray diffraction images are available at the Integrated Resource for Reproducibility in Macromolecular Crystallography at www.proteindiffraction.org.[68] Data were indexed and integrated with HKL2000[69] and scaled with XSCALE.[70] The structure was solved with Phaser[71] using an inhibitor-bound structure of *Pv*NMT (PDB entry 6NXG[33]) as a search model. The model was refined with iterative rounds of automated refinement with Phenix[72] and manual model building with Coot (Table S4).[73] The quality of the structure was checked with MolProbity.[74]

Illustrations. Chemical structures were drawn using Pubsketcher v2.4. Images of molecular structures were produced with the aid of Chimera and PyMol.[75−77] Sequence alignments of *C. parvum* (Iowa II strain) with *Cryptosporidium* and other eukaryotic NMT orthologs were performed using MUSCLE v3.8[78] (Figure 4B) and Clustal Omega[79,80] (Figure S2) and illustrated with ESPript 3.0.[46] UniProt or NCBI accession codes of the aligned sequences are as follows: Q5CV46 (*C. parvum* strain Iowa II NMT), TRY52658.1 (*Cryptosporidium tyzzeri* NMT), XP_667560.1 (*Cryptosporidium hominis* TU502 NMT), OLQ16601.1 (*C. hominis* NMT), A0A2P4Z0T6 (*Cryptosporidium meleagridis* NMT), KAH8584540.1 (*Cryptosporidium* sp. chipmunk genotype I NMT), XP_028874235.1 (*Cryptosporidium ubiquitum* NMT), KAH8742064.1 (*Cryptosporidium ryanae* NMT), KAH7647975.1 (*Cryptosporidium bovis* NMT), B6A985 (*Cryptosporidium muris* RN66 NMT), A0A1J4MZG9 (*Cryptosporidium andersoni* NMT), P14743 (*S. cerevisiae* NMT1), P30418 (*C. albicans* NMT1), Q4Q5S8 (*L. major* NMT), A5K1A2 (*P. vivax* strain Salvador I NMT), O61613 (*Drosophila melanogaster* NMT), A0A1X7VMH8 (*Amphime-*

https://doi.org/10.1021/acsinfecdis.3c00151
ACS Infect. Dis. 2023, 9, 1821−1833

don queenslandica NMT), D2A651 (*Tribolium castaneum* NMT), A0A812BHC6 (*Sep25haraonicnis* NMT), Q4VBR7 (*Danio rerio* NMT1), Q7ZYT2 (*Xenopus laevis* NMT1), J3SCE1 (*Crotalus adamanteus* NMT), P30419 (*H. sapiens* NMT1), A0A1L1RKT0 (*Gallus gallus* NMT1), S4R7E3 (*Petromyzon marinus* NMT), H2ZRH9 (*D. rerio* NMT2), Q6DKD8 (*X. laevis* NMT2), O60551 (*H. sapiens* NMT2), XP_040521574.1 (*G. gallus* NMT2), Q9LTR9 (*Arabidopsis thaliana* NMT1), and A0A2K3DM01 (*Chlamydomonas reinhardtii* NMT).

Synthesis of the New Compound (9). Compound **9** was synthesized following procedures described in a patent for **2** and analogs,[81] as shown in Scheme 1. First, 2-amino-3-nitrobenzoic acid (**10**) and thiazol-2-amine (**11**) were treated with EDCI/HOBT in DCM to generate **12**. After reduction of **12** by $NaBH_4/NiCl_2$, benzimidazole **15** was then obtained by reacting **13** with aldehyde **14** in 82% yield. Finally, the desired **9** was obtained by removing the Boc group in TFA/DCM. Detailed procedures and compound characterization are provided in the Supporting Information.

■ ASSOCIATED CONTENT

Supporting Information

The Supporting Information is available free of charge at https://pubs.acs.org/doi/10.1021/acsinfecdis.3c00151.

Methods for chemical synthesis and protein constructs used in crystallization, figures showing assay optimization results, NMR spectra, NMT amino acid sequence alignments, crystal packing effects, composite omit maps of ligands, and stereoview reproductions of Figures 3 and 5A,B, and tables of protein constructs, DNA primers, X-ray diffraction statistics, and structural refinement data (PDF)

■ AUTHOR INFORMATION

Corresponding Authors

Erkang Fan − *Department of Biochemistry, University of Washington, Seattle, Washington 98195, United States*; Email: erkang@uw.edu

Bart L. Staker − *Seattle Structural Genomics Center for Infectious Disease (SSGCID), Seattle, Washington 98109, United States; Center for Global Infectious Disease Research, Seattle Children's Research Institute, Seattle, Washington 98109, United States*; orcid.org/0000-0001-9570-5086; Email: bart.staker@seattlechildrens.org

Authors

Michael K. Fenwick − *Seattle Structural Genomics Center for Infectious Disease (SSGCID), Seattle, Washington 98109, United States*

Alexandra R. Reers − *Seattle Structural Genomics Center for Infectious Disease (SSGCID), Seattle, Washington 98109, United States; Center for Global Infectious Disease Research, Seattle Children's Research Institute, Seattle, Washington 98109, United States*

Yi Liu − *Department of Biochemistry, University of Washington, Seattle, Washington 98195, United States*; orcid.org/0000-0003-1513-8638

Rachael Zigweid − *Seattle Structural Genomics Center for Infectious Disease (SSGCID), Seattle, Washington 98109, United States; Center for Global Infectious Disease Research, Seattle Children's Research Institute, Seattle, Washington 98109, United States*

Banumathi Sankaran − *Berkeley Center for Structural Biology, Advanced Light Source, Berkeley National Laboratory, Berkeley, California 94720, United States*

Janis Shin − *Seattle Structural Genomics Center for Infectious Disease (SSGCID), Seattle, Washington 98109, United States; Center for Global Infectious Disease Research, Seattle Children's Research Institute, Seattle, Washington 98109, United States*; orcid.org/0000-0002-1657-2455

Matthew A. Hulverson − *Center for Emerging and Re-emerging Infectious Diseases, Division of Allergy and Infectious Diseases, Department of Medicine, University of Washington, Seattle, Washington 98109, United States*; orcid.org/0000-0002-3413-4969

Bradley Hammerson − *Seattle Structural Genomics Center for Infectious Disease (SSGCID), Seattle, Washington 98109, United States; Center for Global Infectious Disease Research, Seattle Children's Research Institute, Seattle, Washington 98109, United States*

Elena Fernández Álvaro − *GSK Global Health, 28760 Madrid, Spain*

Peter J. Myler − *Seattle Structural Genomics Center for Infectious Disease (SSGCID), Seattle, Washington 98109, United States; Center for Global Infectious Disease Research, Seattle Children's Research Institute, Seattle, Washington 98109, United States; Department of Global Health and Department of Pediatrics, University of Washington, Seattle, Washington 98195, United States*

Alexis Kaushansky − *Center for Global Infectious Disease Research, Seattle Children's Research Institute, Seattle, Washington 98109, United States; Center for Emerging and Re-emerging Infectious Diseases, Division of Allergy and Infectious Diseases, Department of Medicine, University of Washington, Seattle, Washington 98109, United States; Department of Global Health, University of Washington, Seattle, Washington 98195, United States*; orcid.org/0000-0001-5721-258X

Wesley C. Van Voorhis − *Seattle Structural Genomics Center for Infectious Disease (SSGCID), Seattle, Washington 98109, United States; Center for Emerging and Re-emerging Infectious Diseases, Division of Allergy and Infectious Diseases, Department of Medicine, University of Washington, Seattle, Washington 98109, United States*

Complete contact information is available at: https://pubs.acs.org/10.1021/acsinfecdis.3c00151

Author Contributions

¶M.K.F. and A.R.R. contributed equally to this work.

Notes

The authors declare no competing financial interest.

■ ACKNOWLEDGMENTS

We thank Dr. Anke Harupa-Chung for assistance and training of A.R.R. in the *N*-myristoyltransferase assay and providing interpretation of assay data. The ALS-ENABLE beamlines are supported in part by the National Institutes of Health (NIH), National Institute of General Medical Sciences, grant P30 GM124169-01. The ALS is a Department of Energy Office of Science User Facility under Contract No. DE-AC02-05CH11231. The SSGCID is supported with Federal funds from the National Institute of Allergy and Infectious Diseases

(NIAID), NIH, Department of Health and Human Services, under Contract numbers HHSN272201700059C and 75N93022C00036. Research reported in this publication was supported by the NIAID of the NIH under award numbers R01AI155536 and R21AI137815.

REFERENCES

(1) https://www.who.int/news-room/fact-sheets/detail/diarrhoeal-disease.

(2) Kotloff, K. L.; Nataro, J. P.; Blackwelder, W. C.; Nasrin, D.; Farag, T. H.; Panchalingam, S.; Wu, Y.; Sow, S. O.; Sur, D.; Breiman, R. F.; Faruque, A. S.; Zaidi, A. K.; Saha, D.; Alonso, P. L.; Tamboura, B.; Sanogo, D.; Onwuchekwa, U.; Manna, B.; Ramamurthy, T.; Kanungo, S.; Ochieng, J. B.; Omore, R.; Oundo, J. O.; Hossain, A.; Das, S. K.; Ahmed, S.; Qureshi, S.; Quadri, F.; Adegbola, R. A.; Antonio, M.; Hossain, M. J.; Akinsola, A.; Mandomando, I.; Nhampossa, T.; Acacio, S.; Biswas, K.; O'Reilly, C. E.; Mintz, E. D.; Berkeley, L. Y.; Muhsen, K.; Sommerfelt, H.; Robins-Browne, R. M.; Levine, M. M. Burden and aetiology of diarrhoeal disease in infants and young children in developing countries (the Global Enteric Multicenter Study, GEMS): a prospective, case-control study. *Lancet* **2013**, *382*, 209−222.

(3) Platts-Mills, J. A.; Babji, S.; Bodhidatta, L.; Gratz, J.; Haque, R.; Havt, A.; McCormick, B. J.; McGrath, M.; Olortegui, M. P.; Samie, A.; Shakoor, S.; Mondal, D.; Lima, I. F.; Hariraju, D.; Rayamajhi, B. B.; Qureshi, S.; Kabir, F.; Yori, P. P.; Mufamadi, B.; Amour, C.; Carreon, J. D.; Richard, S. A.; Lang, D.; Bessong, P.; Mduma, E.; Ahmed, T.; Lima, A. A.; Mason, C. J.; Zaidi, A. K.; Bhutta, Z. A.; Kosek, M.; Guerrant, R. L.; Gottlieb, M.; Miller, M.; Kang, G.; Houpt, E. R.; Investigators, M.-E. N. Pathogen-specific burdens of community diarrhoea in developing countries: a multisite birth cohort study (MAL-ED). *Lancet Glob. Health* **2015**, *3*, e564−e575.

(4) Huston, C. D.; Spangenberg, T.; Burrows, J.; Willis, P.; Wells, T. N.; van Voorhis, W. A proposed target product profile and developmental cascade for new cryptosporidiosis treatments. *PLoS Negl. Trop. Dis.* **2015**, *9*, No. e0003987.

(5) Liu, J.; Platts-Mills, J. A.; Juma, J.; Kabir, F.; Nkeze, J.; Okoi, C.; Operario, D. J.; Uddin, J.; Ahmed, S.; Alonso, P. L.; Antonio, M.; Becker, S. M.; Blackwelder, W. C.; Breiman, R. F.; Faruque, A. S.; Fields, B.; Gratz, J.; Haque, R.; Hossain, A.; Hossain, M. J.; Jarju, S.; Qamar, F.; Iqbal, N. T.; Kwambana, B.; Mandomando, I.; McMurry, T. L.; Ochieng, C.; Ochieng, J. B.; Ochieng, M.; Onyango, C.; Panchalingam, S.; Kalam, A.; Aziz, F.; Qureshi, S.; Ramamurthy, T.; Roberts, J. H.; Saha, D.; Sow, S. O.; Stroup, S. E.; Sur, D.; Tamboura, B.; Taniuchi, M.; Tennant, S. M.; Toema, D.; Wu, Y.; Zaidi, A.; Nataro, J. P.; Kotloff, K. L.; Levine, M. M.; Houpt, E. R. Use of quantitative molecular diagnostic methods to identify causes of diarrhoea in children: a reanalysis of the GEMS case-control study. *Lancet* **2016**, *388*, 1291−1301.

(6) Checkley, W.; Epstein, L. D.; Gilman, R. H.; Black, R. E.; Cabrera, L.; Sterling, C. R. Effects of *Cryptosporidium parvum* infection in Peruvian children: growth faltering and subsequent catch-up growth. *Am. J. Epidemiol.* **1998**, *148*, 497−506.

(7) Korpe, P. S.; Haque, R.; Gilchrist, C.; Valencia, C.; Niu, F.; Lu, M.; Ma, J. Z.; Petri, S. E.; Reichman, D.; Kabir, M.; Duggal, P.; Petri, W. A., Jr. Natural history of cryptosporidiosis in a longitudinal study of slum-dwelling Bangladeshi children: association with severe malnutrition. *PLoS Negl. Trop. Dis.* **2016**, *10*, No. e0004564.

(8) Steiner, K. L.; Ahmed, S.; Gilchrist, C. A.; Burkey, C.; Cook, H.; Ma, J. Z.; Korpe, P. S.; Ahmed, E.; Alam, M.; Kabir, M.; Tofail, F.; Ahmed, T.; Haque, R.; Petri, W. A., Jr.; Faruque, A. S. G. Species of *Cryptosporidia* causing subclinical infection associated with growth faltering in rural and urban Bangladesh: a birth cohort study. *Clin. Infect. Dis.* **2018**, *67*, 1347−1355.

(9) Amadi, B.; Mwiya, M.; Musuku, J.; Watuka, A.; Sianongo, S.; Ayoub, A.; Kelly, P. Effect of nitazoxanide on morbidity and mortality in Zambian children with cryptosporidiosis: a randomised controlled trial. *Lancet* **2002**, *360*, 1375−1380.

(10) Mead, J. R. Prospects for immunotherapy and vaccines against *Cryptosporidium*. *Hum. Vaccin. Immunother.* **2014**, *10*, 1505−1513.

(11) Ryan, U.; Hijjawi, N. New developments in *Cryptosporidium* research. *Int. J. Parasitol.* **2015**, *45*, 367−373.

(12) Abrahamsen, M. S.; Templeton, T. J.; Enomoto, S.; Abrahante, J. E.; Zhu, G.; Lancto, C. A.; Deng, M.; Liu, C.; Widmer, G.; Tzipori, S.; Buck, G. A.; Xu, P.; Bankier, A. T.; Dear, P. H.; Konfortov, B. A.; Spriggs, H. F.; Iyer, L.; Anantharaman, V.; Aravind, L.; Kapur, V. Complete genome sequence of the apicomplexan, *Cryptosporidium parvum*. *Science* **2004**, *304*, 441−445.

(13) Xu, P.; Widmer, G.; Wang, Y.; Ozaki, L. S.; Alves, J. M.; Serrano, M. G.; Puiu, D.; Manque, P.; Akiyoshi, D.; Mackey, A. J.; Pearson, W. R.; Dear, P. H.; Bankier, A. T.; Peterson, D. L.; Abrahamsen, M. S.; Kapur, V.; Tzipori, S.; Buck, G. A. The genome of *Cryptosporidium hominis*. *Nature* **2004**, *431*, 1107−1112.

(14) Sanderson, S. J.; Xia, D.; Prieto, H.; Yates, J.; Heiges, M.; Kissinger, J. C.; Bromley, E.; Lal, K.; Sinden, R. E.; Tomley, F.; Wastling, J. M. Determining the protein repertoire of *Cryptosporidium parvum* sporozoites. *Proteomics* **2008**, *8*, 1398−1414.

(15) Vinayak, S.; Pawlowic, M. C.; Sateriale, A.; Brooks, C. F.; Studstill, C. J.; Bar-Peled, Y.; Cipriano, M. J.; Striepen, B. Genetic modification of the diarrhoeal pathogen *Cryptosporidium parvum*. *Nature* **2015**, *523*, 477−480.

(16) Manjunatha, U. H.; Chao, A. T.; Leong, F. J.; Diagana, T. T. Cryptosporidiosis drug discovery: opportunities and challenges. *ACS Infect. Dis.* **2016**, *2*, 530−537.

(17) Vijayan, K.; Kaushansky, A. Exciting contributions to the *Cryptosporidium* renaissance. *Cell Host Microbe* **2019**, *26*, 5−7.

(18) Wilke, G.; Funkhouser-Jones, L. J.; Wang, Y.; Ravindran, S.; Wang, Q.; Beatty, W. L.; Baldridge, M. T.; VanDussen, K. L.; Shen, B.; Kuhlenschmidt, M. S.; Kuhlenschmidt, T. B.; Witola, W. H.; Stappenbeck, T. S.; Sibley, L. D. A stem-cell-derived platform enables complete *Cryptosporidium* development *in vitro* and genetic tractability. *Cell Host Microbe* **2019**, *26*, 123−134.e8.

(19) Schultz, A. M.; Henderson, L. E.; Oroszlan, S.; Garber, E. A.; Hanafusa, H. Amino terminal myristylation of the protein kinase p60src, a retroviral transforming protein. *Science* **1985**, *227*, 427−429.

(20) Mumby, S. M.; Heukeroth, R. O.; Gordon, J. I.; Gilman, A. G. G-protein alpha-subunit expression, myristoylation, and membrane association in COS cells. *Proc. Natl. Acad. Sci. U. S. A.* **1990**, *87*, 728−732.

(21) Farazi, T. A.; Waksman, G.; Gordon, J. I. The biology and enzymology of protein *N*-myristoylation. *J. Biol. Chem.* **2001**, *276*, 39501−39504.

(22) Matsubara, M.; Nakatsu, T.; Kato, H.; Taniguchi, H. Crystal structure of a myristoylated CAP-23/NAP-22 *N*-terminal domain complexed with Ca2+/calmodulin. *EMBO J.* **2004**, *23*, 712−718.

(23) Zhao, C.; Ma, S. Recent advances in the discovery of *N*-myristoyltransferase inhibitors. *ChemMedChem* **2014**, *9*, 2425−2437.

(24) Boutin, J. A. Myristoylation. *Cell. Signal.* **1997**, *9*, 15−35.

(25) Schlott, A. C.; Holder, A. A.; Tate, E. W. *N*-myristoylation as a drug target in malaria: exploring the role of *N*-myristoyltransferase substrates in the inhibitor mode of action. *ACS Infect. Dis.* **2018**, *4*, 449−457.

(26) Roberts, A. J.; Torrie, L. S.; Wyllie, S.; Fairlamb, A. H. Biochemical and genetic characterization of *Trypanosoma cruzi N*-myristoyltransferase. *Biochem. J.* **2014**, *459*, 323−332.

(27) Frearson, J. A.; Brand, S.; McElroy, S. P.; Cleghorn, L. A.; Smid, O.; Stojanovski, L.; Price, H. P.; Guther, M. L.; Torrie, L. S.; Robinson, D. A.; Hallyburton, I.; Mpamhanga, C. P.; Brannigan, J. A.; Wilkinson, A. J.; Hodgkinson, M.; Hui, R.; Qiu, W.; Raimi, O. G.; van Aalten, D. M.; Brenk, R.; Gilbert, I. H.; Read, K. D.; Fairlamb, A. H.; Ferguson, M. A.; Smith, D. F.; Wyatt, P. G. *N*-myristoyltransferase inhibitors as new leads to treat sleeping sickness. *Nature* **2010**, *464*, 728−732.

(28) Price, H. P.; Menon, M. R.; Panethymitaki, C.; Goulding, D.; McKean, P. G.; Smith, D. F. Myristoyl-CoA:protein *N*-myristoyltransferase, an essential enzyme and potential drug target in kinetoplastid parasites. *J. Biol. Chem.* **2003**, *278*, 7206−7214.

https://doi.org/10.1021/acsinfecdis.3c00151
ACS Infect. Dis. 2023, 9, 1821−1833

(29) Wright, M. H.; Clough, B.; Rackham, M. D.; Rangachari, K.; Brannigan, J. A.; Grainger, M.; Moss, D. K.; Bottrill, A. R.; Heal, W. P.; Broncel, M.; Serwa, R. A.; Brady, D.; Mann, D. J.; Leatherbarrow, R. J.; Tewari, R.; Wilkinson, A. J.; Holder, A. A.; Tate, E. W. Validation of *N*-myristoyltransferase as an antimalarial drug target using an integrated chemical biology approach. *Nat. Chem.* **2014**, *6*, 112−121.
(30) Rodríguez-Hernández, D.; Vijayan, K.; Zigweid, R.; Fenwick, M. K.; Sankaran, B.; Roobsoong, W.; Sattabongkot, J.; Glennon, E. K. K.; Myler, P. J.; Sunnerhagen, P.; Staker, B. L.; Kaushansky, A.; Grøtli, M. Identification of potent and selective *N*-myristoyltransferase inhibitors of *Plasmodium vivax* liver stage hypnozoites and schizonts. *bioRxiv* , DOI: 10.1101/2023.01.27.525941.
(31) Yu, Z.; Brannigan, J. A.; Moss, D. K.; Brzozowski, A. M.; Wilkinson, A. J.; Holder, A. A.; Tate, E. W.; Leatherbarrow, R. J. Design and synthesis of inhibitors of *Plasmodium falciparum N*-myristoyltransferase, a promising target for antimalarial drug discovery. *J. Med. Chem.* **2012**, *55*, 8879−8890.
(32) Schlott, A. C.; Mayclin, S.; Reers, A. R.; Coburn-Flynn, O.; Bell, A. S.; Green, J.; Knuepfer, E.; Charter, D.; Bonnert, R.; Campo, B.; Burrows, J.; Lyons-Abbott, S.; Staker, B. L.; Chung, C. W.; Myler, P. J.; Fidock, D. A.; Tate, E. W.; Holder, A. A. Structure-guided identification of resistance breaking antimalarial *N*-myristoyltransferase inhibitors. *Cell Chem. Biol.* **2019**, *26*, 991−1000.
(33) Harupa, A.; De Las Heras, L.; Colmenarejo, G.; Lyons-Abbott, S.; Reers, A.; Caballero Hernandez, I.; Chung, C. W.; Charter, D.; Myler, P. J.; Fernandez-Menendez, R. M.; Calderon, F.; Palomo, S.; Rodriguez, B.; Berlanga, M.; Herreros-Aviles, E.; Staker, B. L.; Fernandez Alvaro, E.; Kaushansky, A. Identification of selective inhibitors of *Plasmodium N*-myristoyltransferase by high-throughput screening. *J. Med. Chem.* **2020**, *63*, 591−600.
(34) Goncalves, V.; Brannigan, J. A.; Thinon, E.; Olaleye, T. O.; Serwa, R.; Lanzarone, S.; Wilkinson, A. J.; Tate, E. W.; Leatherbarrow, R. J. A fluorescence-based assay for *N*-myristoyltransferase activity. *Anal. Biochem.* **2012**, *421*, 342−344.
(35) Hutton, J. A.; Goncalves, V.; Brannigan, J. A.; Paape, D.; Wright, M. H.; Waugh, T. M.; Roberts, S. M.; Bell, A. S.; Wilkinson, A. J.; Smith, D. F.; Leatherbarrow, R. J.; Tate, E. W. Structure-based design of potent and selective *Leishmania N*-myristoyltransferase inhibitors. *J. Med. Chem.* **2014**, *57*, 8664−8670.
(36) Goncalves, V.; Brannigan, J. A.; Whalley, D.; Ansell, K. H.; Saxty, B.; Holder, A. A.; Wilkinson, A. J.; Tate, E. W.; Leatherbarrow, R. J. Discovery of *Plasmodium vivax N*-myristoyltransferase inhibitors: screening, synthesis, and structural characterization of their binding mode. *J. Med. Chem.* **2012**, *55*, 3578−3582.
(37) Zhang, J. H.; Chung, T. D. Y.; Oldenburg, K. R. A simple statistical parameter for use in evaluation and validation of high throughput screening assays. *J. Biomol. Screen.* **1999**, *4*, 67−73.
(38) Brand, S.; Cleghorn, L. A.; McElroy, S. P.; Robinson, D. A.; Smith, V. C.; Hallyburton, I.; Harrison, J. R.; Norcross, N. R.; Spinks, D.; Bayliss, T.; Norval, S.; Stojanovski, L.; Torrie, L. S.; Frearson, J. A.; Brenk, R.; Fairlamb, A. H.; Ferguson, M. A.; Read, K. D.; Wyatt, P. G.; Gilbert, I. H. Discovery of a novel class of orally active trypanocidal *N*-myristoyltransferase inhibitors. *J. Med. Chem.* **2012**, *55*, 140−152.
(39) Hulverson, M. A.; Choi, R.; McCloskey, M. C.; Whitman, G. R.; Ojo, K. K.; Michaels, S. A.; Somepalli, M.; Love, M. S.; McNamara, C. W.; Rabago, L. M.; Barrett, L. K.; Verlinde, C.; Arnold, S. L. M.; Striepen, B.; Jimenez-Alfaro, D.; Ballell, L.; Fernandez, E.; Greenwood, M. N.; Las Heras, L.; Calderon, F.; Van Voorhis, W. C. Repurposing infectious disease hits as anti-*Cryptosporidium* leads. *ACS Infect. Dis.* **2021**, *7*, 1275−1282.
(40) Goldschmidt, L.; Cooper, D. R.; Derewenda, Z. S.; Eisenberg, D. Toward rational protein crystallization: A Web server for the design of crystallizable protein variants. *Protein Sci.* **2007**, *16*, 1569−1576.
(41) Krissinel, E.; Henrick, K. Secondary-structure matching (SSM), a new tool for fast protein structure alignment in three dimensions. *Acta Crystallogr. D Biol. Crystallogr.* **2004**, *60*, 2256−2268.
(42) Thinon, E.; Serwa, R. A.; Broncel, M.; Brannigan, J. A.; Brassat, U.; Wright, M. H.; Heal, W. P.; Wilkinson, A. J.; Mann, D. J.; Tate, E. W. Global profiling of co- and post-translationally N-myristoylated proteomes in human cells. *Nat. Commun.* **2014**, *5*, 4919.
(43) Dian, C.; Perez-Dorado, I.; Riviere, F.; Asensio, T.; Legrand, P.; Ritzefeld, M.; Shen, M.; Cota, E.; Meinnel, T.; Tate, E. W.; Giglione, C. High-resolution snapshots of human *N*-myristoyltransferase in action illuminate a mechanism promoting *N*-terminal Lys and Gly myristoylation. *Nat. Commun.* **2020**, *11*, 1132.
(44) Kosciuk, T.; Price, I. R.; Zhang, X.; Zhu, C.; Johnson, K. N.; Zhang, S.; Halaby, S. L.; Komaniecki, G. P.; Yang, M.; DeHart, C. J.; Thomas, P. M.; Kelleher, N. L.; Fromme, J. C.; Lin, H. NMT1 and NMT2 are lysine myristoyltransferases regulating the ARF6 GTPase cycle. *Nat. Commun.* **2020**, *11*, 1067.
(45) Brannigan, J. A.; Smith, B. A.; Yu, Z.; Brzozowski, A. M.; Hodgkinson, M. R.; Maroof, A.; Price, H. P.; Meier, F.; Leatherbarrow, R. J.; Tate, E. W.; Smith, D. F.; Wilkinson, A. J. N-myristoyltransferase from *Leishmania donovani*: structural and functional characterisation of a potential drug target for visceral leishmaniasis. *J. Mol. Biol.* **2010**, *396*, 985−999.
(46) Robert, X.; Gouet, P. Deciphering key features in protein structures with the new ENDscript server. *Nucleic Acids Res.* **2014**, *42*, W320−W324.
(47) Bhatnagar, R. S.; Futterer, K.; Farazi, T. A.; Korolev, S.; Murray, C. L.; Jackson-Machelski, E.; Gokel, G. W.; Gordon, J. I.; Waksman, G. Structure of *N*-myristoyltransferase with bound myristoylCoA and peptide substrate analogs. *Nat. Struct. Biol.* **1998**, *5*, 1091−1097.
(48) Wu, J.; Tao, Y.; Zhang, M.; Howard, M. H.; Gutteridge, S.; Ding, J. Crystal structures of *Saccharomyces cerevisiae N*-myristoyltransferase with bound myristoyl-CoA and inhibitors reveal the functional roles of the *N*-terminal region. *J. Biol. Chem.* **2007**, *282*, 22185−22194.
(49) Rackham, M. D.; Brannigan, J. A.; Moss, D. K.; Yu, Z.; Wilkinson, A. J.; Holder, A. A.; Tate, E. W.; Leatherbarrow, R. J. Discovery of novel and ligand-efficient inhibitors of *Plasmodium falciparum* and *Plasmodium vivax N*-myristoyltransferase. *J. Med. Chem.* **2013**, *56*, 371−375.
(50) Mousnier, A.; Bell, A. S.; Swieboda, D. P.; Morales-Sanfrutos, J.; Perez-Dorado, I.; Brannigan, J. A.; Newman, J.; Ritzefeld, M.; Hutton, J. A.; Guedan, A.; Asfor, A. S.; Robinson, S. W.; Hopkins-Navratilova, I.; Wilkinson, A. J.; Johnston, S. L.; Leatherbarrow, R. J.; Tuthill, T. J.; Solari, R.; Tate, E. W. Fragment-derived inhibitors of human *N*-myristoyltransferase block capsid assembly and replication of the common cold virus. *Nat. Chem.* **2018**, *10*, 599−606.
(51) Castrec, B.; Dian, C.; Ciccone, S.; Ebert, C. L.; Bienvenut, W. V.; Le Caer, J. P.; Steyaert, J. M.; Giglione, C.; Meinnel, T. Structural and genomic decoding of human and plant myristoylomes reveals a definitive recognition pattern. *Nat. Chem. Biol.* **2018**, *14*, 671−679.
(52) Yu, Z.; Brannigan, J. A.; Rangachari, K.; Heal, W. P.; Wilkinson, A. J.; Holder, A. A.; Leatherbarrow, R. J.; Tate, E. W. Discovery of pyridyl-based inhibitors of *Plasmodium falciparum N*-myristoyltransferase. *Medchemcomm* **2015**, *6*, 1767−1772.
(53) Goncalves, V.; Brannigan, J. A.; Laporte, A.; Bell, A. S.; Roberts, S. M.; Wilkinson, A. J.; Leatherbarrow, R. J.; Tate, E. W. Structure-guided optimization of quinoline inhibitors of *Plasmodium N*-myristoyltransferase. *Medchemcomm* **2017**, *8*, 191−197.
(54) Olaleye, T. O.; Brannigan, J. A.; Roberts, S. M.; Leatherbarrow, R. J.; Wilkinson, A. J.; Tate, E. W. Peptidomimetic inhibitors of N-myristoyltransferase from human malaria and leishmaniasis parasites. *Org. Biomol. Chem.* **2014**, *12*, 8132−8137.
(55) Corpas-Lopez, V.; Moniz, S.; Thomas, M.; Wall, R. J.; Torrie, L. S.; Zander-Dinse, D.; Tinti, M.; Brand, S.; Stojanovski, L.; Manthri, S.; Hallyburton, I.; Zuccotto, F.; Wyatt, P. G.; De Rycker, M.; Horn, D.; Ferguson, M. A. J.; Clos, J.; Read, K. D.; Fairlamb, A. H.; Gilbert, I. H.; Wyllie, S. Pharmacological validation of N-myristoyltransferase as a drug target in *Leishmania donovani*. *ACS Infect Dis* **2019**, *5*, 111−122.
(56) Kersten, C.; Fleischer, E.; Kehrein, J.; Borek, C.; Jaenicke, E.; Sotriffer, C.; Brenk, R. How to design selective ligands for highly

conserved binding sites: a case study using *N*-myristoyltransferases as a model system. *J. Med. Chem.* **2020**, *63*, 2095−2113.
(57) Forte, B.; Ottilie, S.; Plater, A.; Campo, B.; Dechering, K. J.; Gamo, F. J.; Goldberg, D. E.; Istvan, E. S.; Lee, M.; Lukens, A. K.; McNamara, C. W.; Niles, J. C.; Okombo, J.; Pasaje, C. F. A.; Siegel, M. G.; Wirth, D.; Wyllie, S.; Fidock, D. A.; Baragana, B.; Winzeler, E. A.; Gilbert, I. H. Prioritization of molecular targets for antimalarial drug discovery. *ACS Infect Dis* **2021**, *7*, 2764−2776.
(58) Huggins, D. J.; Sherman, W.; Tidor, B. Rational approaches to improving selectivity in drug design. *J. Med. Chem.* **2012**, *55*, 1424−1444.
(59) Kim, S.; Alsaidan, O. A.; Goodwin, O.; Li, Q.; Sulejmani, E.; Han, Z.; Bai, A.; Albers, T.; Beharry, Z.; Zheng, Y. G.; Norris, J. S.; Szulc, Z. M.; Bielawska, A.; Lebedyeva, I.; Pegan, S. D.; Cai, H. Blocking myristoylation of Src inhibits its kinase activity and suppresses prostate cancer progression. *Cancer Res.* **2017**, *77*, 6950−6962.
(60) Hulverson, M. A.; Vinayak, S.; Choi, R.; Schaefer, D. A.; Castellanos-Gonzalez, A.; Vidadala, R. S. R.; Brooks, C. F.; Herbert, G. T.; Betzer, D. P.; Whitman, G. R.; Sparks, H. N.; Arnold, S. L. M.; Rivas, K. L.; Barrett, L. K.; White, A. C., Jr.; Maly, D. J.; Riggs, M. W.; Striepen, B.; Van Voorhis, W. C.; Ojo, K. K. Bumped-kinase inhibitors for cryptosporidiosis therapy. *J. Infect. Dis.* **2017**, *215*, 1275−1284.
(61) Myler, P. J.; Stacy, R.; Stewart, L.; Staker, B. L.; Van Voorhis, W. C.; Varani, G.; Buchko, G. W. The Seattle Structural Genomics Center for Infectious Disease (SSGCID). *Infect. Disord. Drug Targets* **2009**, *9*, 493−506.
(62) Stacy, R.; Begley, D. W.; Phan, I.; Staker, B. L.; Van Voorhis, W. C.; Varani, G.; Buchko, G. W.; Stewart, L. J.; Myler, P. J. Structural genomics of infectious disease drug targets: the SSGCID. *Acta Crystallogr. Sect. F Struct. Biol. Cryst. Commun.* **2011**, *67*, 979−984.
(63) Bryan, C. M.; Bhandari, J.; Napuli, A. J.; Leibly, D. J.; Choi, R.; Kelley, A.; Van Voorhis, W. C.; Edwards, T. E.; Stewart, L. J. High-throughput protein production and purification at the Seattle Structural Genomics Center for Infectious Disease. *Acta Crystallogr. Sect. F Struct. Biol. Cryst. Commun.* **2011**, *67*, 1010−1014.
(64) Choi, R.; Kelley, A.; Leibly, D.; Hewitt, S. N.; Napuli, A.; Van Voorhis, W. Immobilized metal-affinity chromatography protein-recovery screening is predictive of crystallographic structure success. *Acta Crystallogr. Sect. F Struct. Biol. Cryst. Commun.* **2011**, *67*, 998−1005.
(65) Serbzhinskiy, D. A.; Clifton, M. C.; Sankaran, B.; Staker, B. L.; Edwards, T. E.; Myler, P. J. Structure of an ADP-ribosylation factor, ARF1, from *Entamoeba histolytica* bound to Mg(2+)-GDP. *Acta Crystallogr. F Struct. Biol. Commun.* **2015**, *71*, 594−599.
(66) Aslanidis, C.; de Jong, P. J. Ligation-independent cloning of PCR products (LIC-PCR). *Nucleic Acids Res.* **1990**, *18*, 6069−6074.
(67) Studier, F. W. Protein production by auto-induction in high density shaking cultures. *Protein Expression Purif.* **2005**, *41*, 207−234.
(68) Grabowski, M.; Cymborowski, M.; Porebski, P. J.; Osinski, T.; Shabalin, I. G.; Cooper, D. R.; Minor, W. The Integrated Resource for Reproducibility in Macromolecular Crystallography: Experiences of the first four years. *Struct. Dyn.* **2019**, *6*, No. 064301.
(69) Otwinowski, Z.; Minor, W. Processing of X-ray diffraction data collected in oscillation mode. *Methods Enzymol.* **1997**, *276*, 307−326.
(70) Kabsch, W. XDS. *Acta Crystallogr. D Biol. Crystallogr.* **2010**, *66*, 125−132.
(71) McCoy, A. J.; Grosse-Kunstleve, R. W.; Adams, P. D.; Winn, M. D.; Storoni, L. C.; Read, R. J. *Phaser* crystallographic software. *J. Appl. Crystallogr.* **2007**, *40*, 658−674.
(72) Adams, P. D.; Afonine, P. V.; Bunkoczi, G.; Chen, V. B.; Davis, I. W.; Echols, N.; Headd, J. J.; Hung, L. W.; Kapral, G. J.; Grosse-Kunstleve, R. W.; McCoy, A. J.; Moriarty, N. W.; Oeffner, R.; Read, R. J.; Richardson, D. C.; Richardson, J. S.; Terwilliger, T. C.; Zwart, P. H. PHENIX: a comprehensive Python-based system for macromolecular structure solution. *Acta Crystallogr. D Biol. Crystallogr.* **2010**, *66*, 213−221.
(73) Emsley, P.; Lohkamp, B.; Scott, W. G.; Cowtan, K. Features and development of Coot. *Acta Crystallogr. D Biol. Crystallogr.* **2010**, *66*, 486−501.
(74) Chen, V. B.; Arendall, W. B., 3rd; Headd, J. J.; Keedy, D. A.; Immormino, R. M.; Kapral, G. J.; Murray, L. W.; Richardson, J. S.; Richardson, D. C. MolProbity: all-atom structure validation for macromolecular crystallography. *Acta Crystallogr. D Biol. Crystallogr.* **2010**, *66*, 12−21.
(75) *The PyMOL Molecular Graphics System, Version 2.0* Schrödinger, LLC.
(76) Pettersen, E. F.; Goddard, T. D.; Huang, C. C.; Couch, G. S.; Greenblatt, D. M.; Meng, E. C.; Ferrin, T. E. UCSF Chimera–a visualization system for exploratory research and analysis. *J. Comput. Chem.* **2004**, *25*, 1605−1612.
(77) Meng, E. C.; Pettersen, E. F.; Couch, G. S.; Huang, C. C.; Ferrin, T. E. Tools for integrated sequence-structure analysis with UCSF Chimera. *BMC Bioinformatics* **2006**, *7*, 339.
(78) Edgar, R. C. MUSCLE: multiple sequence alignment with high accuracy and high throughput. *Nucleic Acids Res.* **2004**, *32*, 1792−1797.
(79) Sievers, F.; Wilm, A.; Dineen, D.; Gibson, T. J.; Karplus, K.; Li, W.; Lopez, R.; McWilliam, H.; Remmert, M.; Soding, J.; Thompson, J. D.; Higgins, D. G. Fast, scalable generation of high-quality protein multiple sequence alignments using Clustal Omega. *Mol. Syst. Biol.* **2011**, *7*, 539.
(80) Madeira, F.; Pearce, M.; Tivey, A. R. N.; Basutkar, P.; Lee, J.; Edbali, O.; Madhusoodanan, N.; Kolesnikov, A.; Lopez, R. Search and sequence analysis tools services from EMBL-EBI in 2022. *Nucleic Acids Res.* **2022**, *50*, W276−W279.
(81) Vu, C. B.; Disch, J. S.; Ng, P. Y.; Blum, C. A.; Perni, R. B. Benzimidazoles and related analogs as sirtuin modulators. WO 2010003048 A1, January 7, 2010.

https://doi.org/10.1021/acsinfecdis.3c00151
ACS Infect. Dis. 2023, 9, 1821−1833